JACS
JOURNAL OF THE AMERICAN CHEMICAL SOCIETY
pubs.acs.org/JACS
Article

Peristaltic Motion in Structurally Adaptive Molecular Crystals Enables Selective Propyne Capture

Yun-Hsien Lin,[#] Hayden A. Evans,[#] Asif Raza, Sousa Javan Nikkhah, Xia Li, Michael J. Zaworotko, Matthias Vandichel, Soumya Mukherjee,[*] and Ognjen Š. Miljanić[*]

Cite This: J. Am. Chem. Soc. 2025, 147, 43957−43963
Read Online

ACCESS | Metrics & More | Article Recommendations | Supporting Information

ABSTRACT: Cyclotetrabenzoin and its tetraacetate, two macrocyclic porous molecular crystals, were examined as adsorbents for light hydrocarbons, with a focus on C_3 hydrocarbons: propane, propene, and propyne. While both materials exhibit a preference for propyne, only the tetraacetate—owing to its higher surface area (570 vs. 42 $m^2\ g^{-1}$), enhanced uptake capacity (1.99 vs. 1.19 mmol g^{-1}), and faster kinetics—achieves dynamic binary separation of propyne from propylene under ambient conditions and various influent ratios (1/1, 1/2, and 2/1, *v*/*v*). The high propyne selectivity and separation trends were explained by using a combination of *in situ* synchrotron powder X-ray diffraction and molecular dynamics. These techniques suggested that the more rigid, extensively hydrogen-bonded structure of cyclotetrabenzoin transports propyne chiefly through pore enlargement. In cyclotetrabenzoin acetate, the absence of hydrogen bonding and larger void volume (25.9 vs. 9.6% in cyclotetrabenzoin) allows extensive structural adaptation that facilitates the capture and transport of propyne through the crystal. Rotation of cyclotetrabenzoin acetate's benzene aromatic panels by ≈19° allows adjustment to the propyne structure, maximizing interactions with the C≡C triple bond and the acetylenic hydrogen. Beyond the molecule, extensive fluxionality allows for peristaltic transport of guests through the material but can also result in transient closure of one-dimensional channels observed in the single-crystal X-ray structure. These results highlight the importance of subtle structural adaptations in sorbent structures to the bulk separation performance and offer a new design strategy for gas sorption in transiently porous and ultramicroporous molecules.

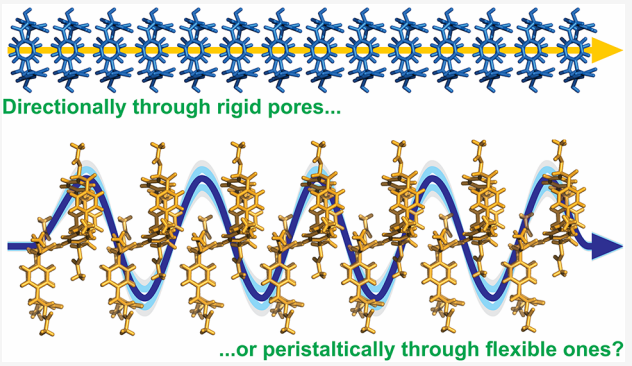

INTRODUCTION

The global chemical industry generated an estimated annual revenue of about $6.2 trillion in 2024 (excluding pharmaceuticals), representing roughly 5.4% of the global GDP. At the same time, the chemical industry is the largest energy consumer among all of the industrial sectors (8.5 Quad in 2022) and the third largest direct emitter of CO_2 (935 Mt in 2022).[1] As the demand for chemical raw materials and plastics keeps increasing, these figures are projected to rise. Within the chemical industry, energy-intensive distillation-based separations of raw materials and products consume about 15% of all of the energy used in the United States.[2] Switching some or all of these distillation-based separations to membrane-based alternatives could save as much as 90% of energy currently used in this sector. This is especially salient in the immensely important large-scale separations of ethylene and propylene from their alkane and alkyne relatives, as these gaseous mixtures lend themselves well to membrane-based separations.[3]

Propylene (C_3H_6) is an essential building block for polypropylene and other commodity chemicals, but industrial feeds inevitably contain trace propyne (C_3H_4) that poisons polymerization catalysts. Polymer-grade (99.9995%) propylene therefore requires C_3H_4 contents below a few parts per million. The conventional remedy—selective hydrogenation of propyne/propylene mixtures over noble metal catalysts—is expensive and plagued by short catalyst lifetimes and secondary pollution. To address this shortcoming, adsorptive purification using reticular porous sorbents is emerging as a more energy-efficient alternative to cryogenic distillation. Traditional adsorbents such as zeolites and activated carbons cannot discriminate between C_3H_4 and C_3H_6 because of their similar size and polarity; in contrast, metal−organic frameworks (MOFs) with ultramicroporous (pore aperture <7 Å) channels and functional groups have recently come to the fore, offering

Received: September 19, 2025
Revised: November 10, 2025
Accepted: November 12, 2025
Published: November 17, 2025

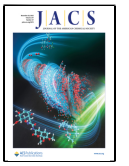

https://doi.org/10.1021/jacs.5c16526
J. Am. Chem. Soc. 2025, 147, 43957−43963

strong yet selective C_3H_4 binding. Early flexible frameworks such as **ELM-12**, $[Cu(bpy)_2(triflate)_2]_n$ delivered propylene purity above 99.999% via confinement-driven C_3H_4 binding.[4] Interpenetrated hybrid ultramicroporous materials (HUMs) like **TIFSIX-14-Cu-i**, $[Cu(14)_2(TiF_6)]_n$ (TIFSIX = TiF_6^{2-}, 14 = 4,4′-azobipyridine, *i* = interpenetrated) feature anion-pillared ≈3.4 Å pores and capture C_3H_4 at sub-0.1 bar, producing polymer-grade propylene. MOFs with more open pores (on the order of ≈5.7 Å), **NKMOF-1-M**, and $Cu[M(pdt)_2]_n$ (*pdt* = pyrazine-2,3-dithiol; M = Cu, Ni) combine hydrogen bonding and $[\pi\cdots\pi]$ stacking to attain very high selectivity. However, strong sorbate−framework interactions raise regeneration energies and limit working capacity, so a balance of interaction energetics is a significant consideration. A forward-looking strategy is to design structurally adaptive physisorbents in which guest-triggered flexibility provides high selectivity at low pressures while opening additional porosity at higher loadings.[5] Responsive and structurally adaptive physisorbents that offer induced-fit binding selective to propyne could thus break the long-standing trade-off between selectivity and working capacity (*i.e.*, uptake), and deliver energy-efficient C_3H_4/C_3H_6 separations.

Among organic porous materials, covalent organic frameworks (COFs)[6] and ultramicroporous polymers[7] have been used for the separations of C_2 and C_3 hydrocarbons. Solution-processable porous molecular crystals (PMCs)[8] have been studied less in this context. Predicated upon a symmetric C_{24} macrocyclic core, here we present a pair of PMCs, cyclotetrabenzoin (**CTBZ**) and cyclotetrabenzoin acetate (**CTBZ-A**), which exhibit high selectivity for propyne over propylene and propane (C_3H_8). These propyne selectivities result in the more porous **CTBZ-A** efficiently separating propyne from propylene, and are underpinned by the specific interactions of the triple bond of propyne with the four aromatic walls of the narrow cavity in **CTBZ** and **CTBZ-A**, a bespoke insight obtained from *in situ* synchrotron powder X-ray diffraction and molecular dynamics (MD). This study presents a detailed blueprint on interpreting and utilizing minute differences in molecular structure to affect propyne affinity, framework flexibility, and ultimately bulk sorption behavior.

RESULTS AND DISCUSSION

The **CTBZ** macrocycle (Figure 1, top left) was first prepared in 2015 through a cyanide-catalyzed benzoin condensation of terephthaldehyde.[9] Its X-ray crystal structure shows molecules of **CTBZ** organized into perfectly aligned nanotubes, stabilized by an extensive network of strong hydrogen bonds between the carbonyl and hydroxy oxygens on one molecule of **CTBZ** and the hydroxyl hydrogens on another (Figure 1, bottom left). In contrast, acetylated cyclotetrabenzoin **CTBZ-A** (Figure 1, top right)[10] lacks the ability to hydrogen bond to itself, which makes it more soluble in organic solvents than **CTBZ**. In the solid state, **CTBZ-A** is unable to efficiently pack, which creates secondary, larger, diamond-shaped voids (Figure 1, bottom right). Both **CTBZ** and **CTBZ-A** are thermally stable, air-stable, and phase-pure bulk solids (Figures S1−S4), which can readily be produced in multigram quantities with uniform particle size distribution (Figures S5−S9). **CTBZ** was found to be hydrophobic (Figure S10) with cryogenic N_2 (77 K) and CO_2 (195 K) adsorption isotherms revealing low Brunauer−Emmett−Teller (BET) surface areas of 42 and 174 $m^2\ g^{-1}$, respectively (Figures S11 and S12). **CTBZ-A** is dramatically more porous, with BET surface areas of 570 and 461 $m^2\ g^{-1}$

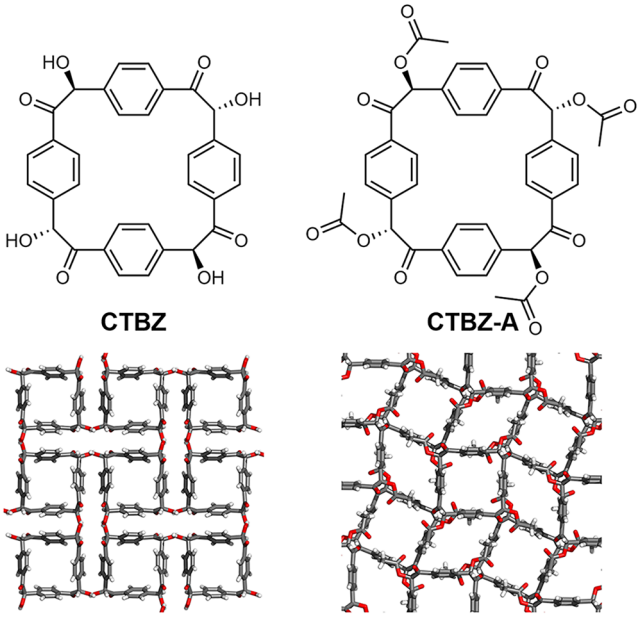

Figure 1. On the top are the structures of cyclotetrabenzoin (**CTBZ**) and cyclotetrabenzoin acetate (**CTBZ-A**). On the bottom are segments of crystal packing diagrams of **CTBZ** (left) and **CTBZ-A** (right), viewed along their respective crystallographic *c* axes.

derived from the N_2 (77 K) and CO_2 (195 K) adsorption isotherms, respectively (Figures S11 and S12). Calculated surface areas from single-crystal structures (using a 2.2 Å probe) are 53 $m^2\ g^{-1}$ for **CTBZ** and 576 $m^2\ g^{-1}$ for **CTBZ-A**. Increased porosity of **CTBZ-A** is attributed to the combination of intrinsic porosity of the macrocycle and its extrinsic porosity stemming from the inability to pack efficiently in the solid state. Improved processability and higher porosity of **CTBZ-A** have allowed its use in lithium−sulfur batteries,[11] separation of CO_2 from CH_4, N_2,[12] and CO,[13] and capture of terminal alkynes and nitriles.[14]

Powder X-ray diffraction (PXRD) was employed to confirm the bulk phase purity of both **CTBZ** and **CTBZ-A** (Figure S1). Thermogravimetric analysis (TGA) showed thermal decomposition occurring at 350 and 310 °C for **CTBZ** and **CTBZ-A**, respectively (Figure S2). Differential scanning calorimetry (DSC) traces collected at 3 °C min^{-1} show a clear melting endotherm for **CTBZ** at ≈220 °C and for **CTBZ-A** at 237 °C. Each material then exhibits a pronounced thermal event attributed to decomposition at 314 °C for **CTBZ** and ≈270 °C for **CTBZ-A** (Figures S3 and S4). These decomposition temperatures coincide with the onset of mass loss in TGA, defining the thermal stability limits of the two solids.

As **CTBZ** and **CTBZ-A** were both found to be robust, readily scalable adsorbents, we evaluated their ambient-temperature gas sorption performances, focusing on CO_2 and the C_2 and C_3 hydrocarbons (Figures S12−S36). Because of its low surface area, **CTBZ** has thus far not been applied in gas sorption experiments. Initial C_2 hydrocarbon gas sorption experiments were conducted at 25 °C (298 K) and showed preferred sorption of acetylene (C_2H_2) relative to ethylene (C_2H_4) and ethane (C_2H_6) in both **CTBZ** and **CTBZ-A** (Figures S23 and S24), but with approximately seven times higher C_2H_2 capacity in **CTBZ-A** (2.16 vs. 0.28 mmol g^{-1}). As the temperature was lowered to 0 °C, capacities increased in both materials; but lowered the C_2H_2 capacity preference for

https://doi.org/10.1021/jacs.5c16526
J. Am. Chem. Soc. 2025, 147, 43957−43963

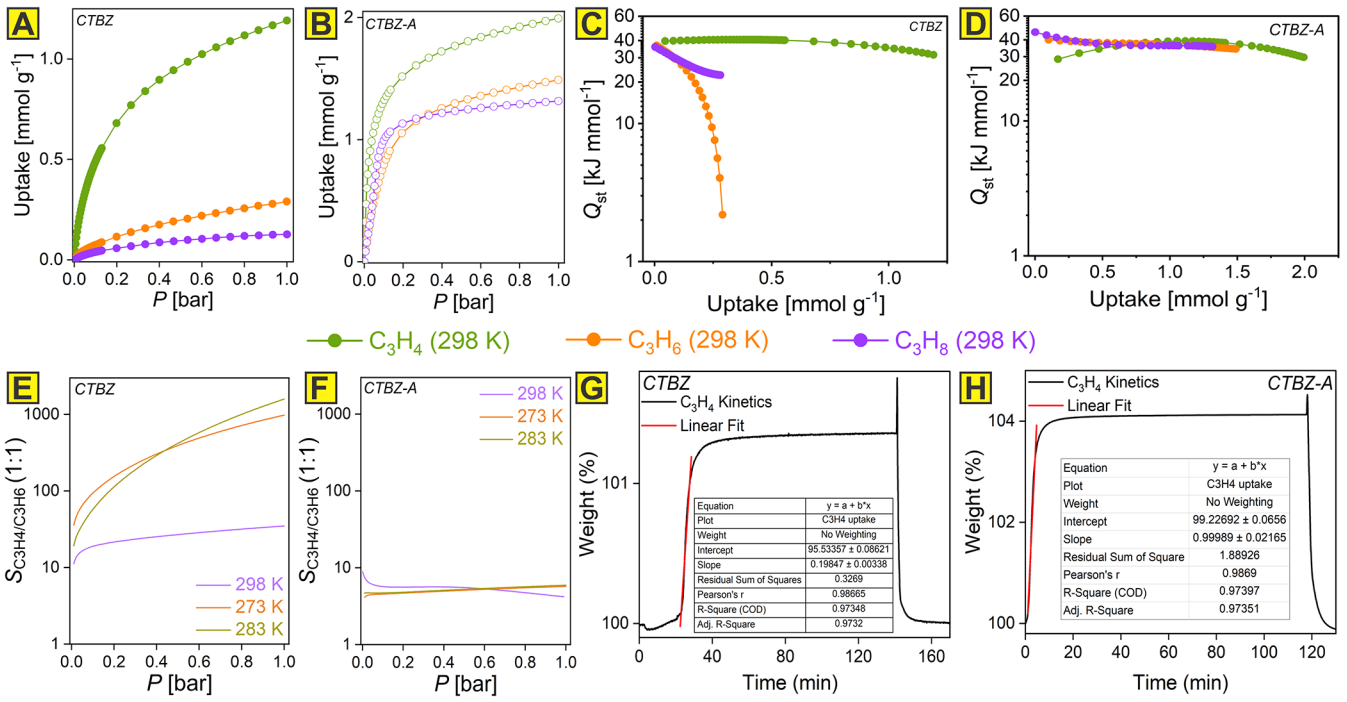

Figure 2. C_3 gas adsorption isotherms recorded at 298 K for **CTBZ** (A) and **CTBZ-A** (B). C_3 isosteric enthalpy of adsorption profiles for **CTBZ** (C) and **CTBZ-A** ((D) olive green: C_3H_4; orange: C_3H_6; purple: C_3H_8). Selectivity for C_3H_4 over C_3H_6 ($S_{C3H4/C3H6}$) in a 1:1 *v*/*v* mixture across loadings, up to 1 bar, was determined from pure C_3 gas sorption isotherms using IAST, for **CTBZ** (E) and **CTBZ-A** (F). C_3H_4 adsorption kinetics analysis at 303 K was carried out for **CTBZ** (G) and **CTBZ-A** (H).

CTBZ-A over **CTBZ** to three times: 3.42 vs. 1.01 mmol g^{-1}. From the virial fit of isotherms recorded at 298, 283, and 273 K, the isosteric enthalpy of C_2H_2 adsorption, $Q_{st}(C_2H_2)$, values of 35.8 and 34.0 kJ mol^{-1} were determined for **CTBZ** and **CTBZ-A** (Figures S40 and S42), respectively. Ideal Adsorbed Solution Theory (IAST) revealed that both **CTBZ** and **CTBZ-A** have a very slight preference for CO_2 over C_2H_2 (Figures S25 and S26), consistent with the comparable $Q_{st}(CO_2)$ of 34.1 kJ mol^{-1} determined for **CTBZ-A** (Figure S38). Switching to C_3 hydrocarbons, *viz.*, propyne, propylene, and propane, revealed similar C_3H_4-selective trends but much more pronounced differences in the sorption capacities for **CTBZ** and **CTBZ-A**. At 298 K, **CTBZ** adsorbed 1.2 mmol g^{-1} of C_3H_4 (Figure 2A), contrary to the significantly smaller amounts of both propylene (0.2 mmol g^{-1}) and propane (0.1 mmol g^{-1}). Conversely, **CTBZ-A** registered higher capacities for all three gases (Figure 2B). As a result, at 298 K and 1 bar, the C_3H_4/C_3H_6 uptake ratio registered by **CTBZ** (4.10) was found to be higher than that in **CTBZ-A** (1.34). Lowering the temperature to 283 and then 273 K led to increased capacities for all C_3 gases in both sorbents (Figures S27−S36), but with C_3H_4/C_3H_6 uptake ratios and IAST selectivities improving in **CTBZ** and eroding in **CTBZ-A** (Figure 2E,F; Table S2). Isosteric enthalpies of adsorption, $Q_{st}(C_3H_4)$, $Q_{st}(C_3H_6)$, and $Q_{st}(C_3H_8)$ were determined to be 36−40 kJ mol^{-1} for **CTBZ** and 29−46 kJ mol^{-1} (for **CTBZ-A**) (Figures 2C,D and S37−S48; Table S1). Further, all three C_3 sorbates' adsorption kinetics were recorded gravimetrically, whereby activated **CTBZ** and **CTBZ-A** were exposed to a constant flow of pure gas at 303 K (∼1 bar, Figures 2G,H and S59−S62). The order of C_3H_4 uptake at equilibrium, evident from the linear kinetic slopes of 0.99 (**CTBZ-A**) ≫ 0.19 (**CTBZ**) and the C_3H_4 adsorption uptakes (5.5 *wt* % in **CTBZ-A** > 1.1 wt % in **CTBZ**), were highly in favor of **CTBZ-A** over **CTBZ**.

CTBZ and **CTBZ-A** exhibit high uptake ratios and IAST selectivities for C_3H_4/C_3H_6, comparable to reported sorbents (Table S2).[15] However, such single-component isotherm-based predictions often overestimate mixed-gas separation performance because kinetic effects, framework flexibility, potential material dynamics, coadsorption, and particle morphology all can impact the isotherms in a way that no longer allows for a detailed analysis by IAST.[16] Such isotherm-based predictions often diverge from mixed-gas separations conducted under flow conditions.[17] Therefore, single-component isotherms and relative adsorption capacities for C_3H_4/C_3H_6 serve as early indicators. Dynamic column breakthrough (DCB) experiments, which directly probe multicomponent mixtures, can quantify separation behavior with much higher accuracy. Accordingly, DCB tests were performed on **CTBZ** and **CTBZ-A** using three inlet gas mixtures of C_3H_4/C_3H_6 in volumetric ratios of 1:2, 1:1, and 2:1. Each bed, contained in an 8 mm-diameter quartz tube and holding ca. 0.55 g of sorbent, received the mixtures at a total flow rate of 1 cm^3 min^{-1}. Before each run, the sorbents were activated at 323 K under the flow of pure He (20 cm^3 min^{-1}), cooled to 298 K, and then used for DCB measurements; eluted gases were analyzed by gas chromatography (Figure S63). Figure 3 shows the time-dependent effluent concentration profiles for C_3H_4 and C_3H_6 exiting **CTBZ-A**. For the three dry binary mixtures under the foregoing DCB conditions, only **CTBZ-A** effected a clear separation, while **CTBZ** afforded coelution of the gases.

Propylene eluted from **CTBZ-A** at 10.0 min g^{-1} in the case of a 1:2 mixture with propyne, 9.75 min g^{-1} in the case of a 1:1 mixture, and 6.6 min g^{-1} in the case of a 2:1 mixture. Propyne eluted later at 29.75 (1:2 mixture), 32.73 (1:1 mixture), and 22.98 (2:1 mixture) min g^{-1}. The difference between the

https://doi.org/10.1021/jacs.5c16526
J. Am. Chem. Soc. 2025, 147, 43957−43963

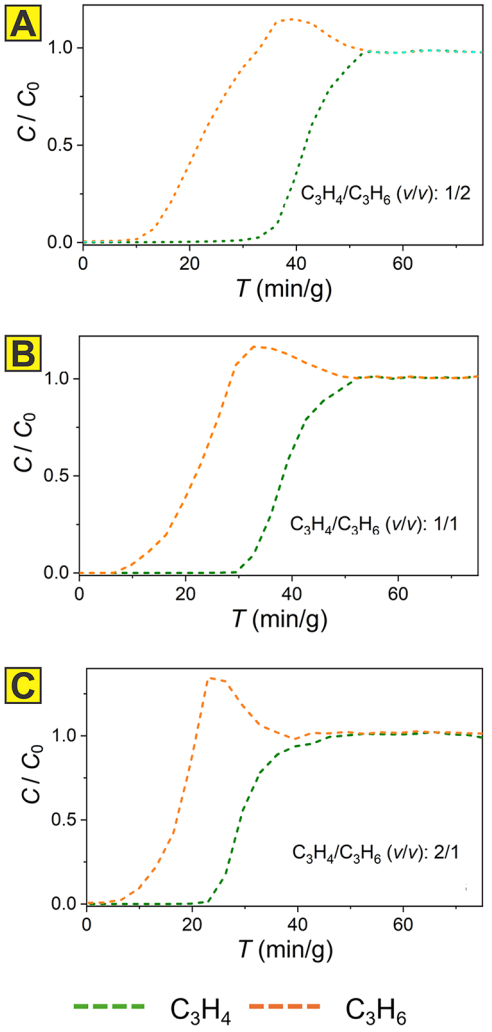

Figure 3. DCB traces at 298 K and 1 bar for the separation of 1:2 (A), 1:1 (B), and 2:1 (C) binary mixtures of C_3H_4/C_3H_6 on **CTBZ-A**.

propyne and propylene breakthrough times was the highest for the 1:1 mixture in the DCB experiments at 22.98 min g^{-1}. Equilibrium mixed-gas uptakes calculated from these DCB data were 15.48 $cm^3\ g^{-1}$ for C_3H_4 (1:2), and 6.69 $cm^3\ g^{-1}$ for C_3H_6 in the 1:2 mixture; 24.73 $cm^3\ g^{-1}$ for C_3H_4 and 9.37 $cm^3\ g^{-1}$ for C_3H_6 in the 1:1 mixture, and 26.58 $cm^3\ g^{-1}$ for C_3H_4 and 8.39 $cm^3\ g^{-1}$ for C_3H_6 in the 2:1 mixture. Overall separation factors of 4.62, 2.64, and 1.58 were determined for the 1:2, 1:1, and 2:1 mixtures, respectively (Figures S64–S69).

To gain a deeper understanding of the binding sites of the gas, we turned to crystallography. Attempts to grow single cocrystals of **CTBZ** and **CTBZ-A** with flammable propyne gas proved technically challenging. Therefore, we used *in situ* synchrotron powder X-ray diffraction of propyne-loaded samples of **CTBZ** and **CTBZ-A** to arrive at their crystal structures after Rietveld refinement (Figures 4 and S70–S83, including adsorption of CO_2 into **CTBZ**). As summarized in Figure S71, as **CTBZ** and **CTBZ-A** are exposed to increasing pressure of propyne, more propyne is found within the crystal structures. To confirm whether our obtained chemical models (propyne positioning) and refined quantities were reasonable, they were compared to experimental isotherm values. As can be seen in Figure S71, the obtained crystallographic occupancies for propyne (refined, not constrained) align well

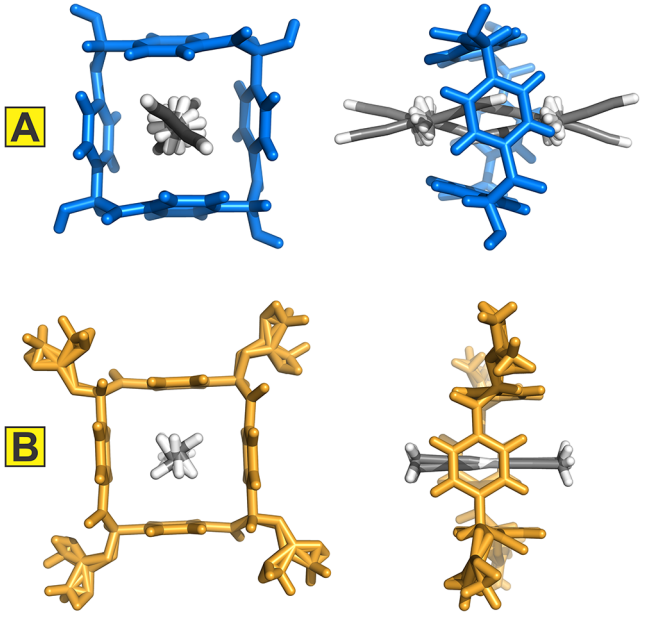

Figure 4. Top (left) and side (right) views of the crystal structures of propyne-loaded **CTBZ** ((A) 1900 Torr) and **CTBZ-A** ((B) 1500 Torr), obtained by *in situ* synchrotron powder X-ray diffraction (28-ID-2, Brookhaven National Laboratory). In both hosts, propyne guest molecules are disordered over several orientations. Element colors: C—gray, H—white. For clarity, the **CTBZ** host is shown in blue and **CTBZ-A** in orange.

with experimental isotherm values. This, alongside the excellent fits to the data made over the multiple pressure ranges for both **CTBZ** and **CTBZ-A**, Figures S74–S83, suggests our chemical models for adsorbed propyne are robust.

Evident in both the **CTBZ** and **CTBZ-A** refined structures is the inclusion of the propyne's C≡C bond into the cavity of the cyclotetrabenzoin macrocycle, with the methyl group residing in the interstitial space between the neighboring molecules of **CTBZ**/**CTBZ-A**, as well as the disorder in the included propyne molecules (Figure 4). This mode of binding parallel that observed for other terminal alkynes and linear guests, with the [$\pi\cdots\pi$] interactions between the triple bond and the aromatic rings of **CTBZ**/**CTBZ-A** playing the key role.[10,13] In **CTBZ-A**, propyne was not observed in the diamond-shaped cavity. Given the larger interstitial space of **CTBZ-A** and the lack of hydrogen bonding between macrocycles, **CTBZ-A** is more readily able to expand and accommodate more adsorbed gas, explaining its higher capacity for propyne vs. **CTBZ**.

Closer examination of the crystal structure of two propyne-loaded hosts reveals subtle but important differences in their geometry. In **CTBZ**, the aromatic panels rotate a bit—from 40.8° in the single-crystal structure[9a] to 37.0° in an evacuated sample, and finally 31.4° in the propyne-loaded samples. In **CTBZ-A**, the aromatic panels are much more flexible: the interplanar angle of 21.2° observed in the single-crystal structure[10,12] changes to 10.1° in the evacuated structure, and the panels become effectively parallel (2.1°) upon loading with propyne. These geometrical changes result in the *de facto* shrinking of the aperture in **CTBZ** to roughly 6.0 Å, whereas for **CTBZ-A** it remains more open at ≈7.0 Å (measured as the shortest distance between a pair of hydrogen atoms on phenylene rings on the opposite sides of the macrocycles, consistent with the Horvath–Kawazoe (H–K) pore size

https://doi.org/10.1021/jacs.5c16526
J. Am. Chem. Soc. 2025, 147, 43957–43963

distribution profiles-led pore apertures of (≈ 6 Å, Figure S13) obtained from the CO_2 adsorption isotherms at 195 K, Figure S12). This difference in geometry may result in a more "snug" fit of propyne in the **CTBZ**'s cavity.

Geometric trends observed on propyne-loaded samples are consistent with the CO_2-loaded structure of **CTBZ**, with interplanar angles of 37.5° (Figure S73), and the previously reported single-crystal structures of CO_2-loaded **CTBZ-A**, where the corresponding interplanar angles were 18.1−21.3°.[12] However, the CO_2 molecules' center of mass was observed to be symmetrically positioned within the cavity of **CTBZ**/**CTBZ-A**, likely as a consequence of its lower polarity and the steric bulk of propyne's methyl group.

Molecular dynamics calculations provided further insights into the selectivity and transport of propyne and propylene guests through the pores of the two hosts. Modeled over 5 ps (5×10^5 steps) with a time step of 0.01 fs at 298 K, the unit cell volume of **CTBZ** expands by as much as ∼7% (Figure S87), in turn increasing the free volume and surface area (Figure S89a). Nevertheless, the hydrogen-bonded square grid structure (shown in Figure 1, bottom right) never breaks down, suggesting that **CTBZ** is a rigid, low-porosity structure. In contrast, while **CTBZ-A** undergoes almost similar volume expansion, its extended structure is dramatically more flexible on account of the absence of intermolecular hydrogen bonding as well as the free rotations and vibrations of its acyl groups in the empty pore space. The results of this flexibility are highly fluxional stacks of **CTBZ-A** molecules that at times lose long-range order, and the sliding of parallel $x-y$ planes, which can close one-dimensional z-direction channels, leaving only $x-y$ planar pores accessible (Figures S88 and 89b). These features may also explain the marginal discrepancy of the high Q scattering data versus the fit of powder X-ray patterns of **CTBZ-A** (vs. those of **CTBZ**). Regardless, even with minor imperfections in the fits for **CTBZ-A**, the refined propyne positions are chemically rational, and the occupancies are consistent with isotherms, lending credence to our structural conclusions.

The differences in the flexibility of channels in **CTBZ** and **CTBZ-A** directly translate into differences in the transport mechanism and selectivities of the hosts. In the rigid **CTBZ** structure, pore enlargement plays a key role in the adsorption and transport of the propyne guest through the material. The more flexible **CTBZ-A** dramatically changes its channel shape as the guest traverses through it, effectively pushing it through somewhat regardless of the shape. This peristaltic motion through the PMC increases capacity and most likely speeds up transport but lowers the C_3H_4/C_3H_6 selectivity (Figure S86). In ultramicroporous materials, given that adsorbed molecules are commensurate in size with the pore apertures and cavities which they must traverse, these subtle structural movements and rearrangements prove key to the separations of chemically similar gases, especially as a function of transport kinetics.[18]

In conclusion, we have compared **CTBZ** and **CTBZ-A**—two readily scalable cyclotetrabenzoin-based hosts—as adsorbents for C_2 and C_3 gases. **CTBZ** showed superb selectivity for propyne, which was explained by (a) the tighter fit of C_3H_4 among the rotated aromatic panels, (b) higher rigidity of this framework, which lowered the affinity for the less well-suited propylene guest, and (c) the single shape of pores, which prevented the erosion of selectivity. Nevertheless, the very low capacity of **CTBZ** resulted in a material that effectively does not separate propyne from propylene. Instead, **CTBZ-A**, despite its lower selectivity, has proven to be a competent agent for propyne-propylene separation in dynamic column breakthrough experiments. When benchmarked against MOFs and other reticular C_3H_4-selective sorbents, both **CTBZ** and **CTBZ-A** exhibit the characteristic combination of high selectivity and low capacity under ambient conditions (298 K and 1 bar), typical of ultramicroporous physisorbents that are not molecular sieves.[3a] The trade-off between selectivity and capacity is a general point to explore in future studies.[19] Our study highlights the impact of a confluence of subtle structural elements (torsion angles, hydrogen bonding, and interstitial spaces) on the bulk separation performance of porous molecular crystals. It additionally provides computational insights into the relevance of intermolecular motion in gas sorption within soft and transiently porous molecular crystals.[20]

■ ASSOCIATED CONTENT

Supporting Information

The Supporting Information is available free of charge at https://pubs.acs.org/doi/10.1021/jacs.5c16526.

Experimental and computational details, crystallographic information files (PDF)

Molecular dynamic movie 1 (MP4)

Molecular dynamic movie 2 (MP4)

Molecular dynamic movie 3 (MP4)

Molecular dynamic movie 4 (MP4)

■ AUTHOR INFORMATION

Corresponding Authors

Soumya Mukherjee − *Department of Chemical Sciences, Bernal Institute and Research Ireland Centre for Pharmaceuticals (SSPC), University of Limerick, Limerick V94 T9PX, Ireland;* orcid.org/0000-0003-2375-7009; Email: soumya.mukherjee@ul.ie

Ognjen Š. Miljanić − *Department of Chemistry, University of Houston, Houston, Texas 77204-5003, United States; Faculty of Chemical Engineering, Industrial University of Ho Chi Minh City, Ho Chi Minh City 700000, Vietnam;* orcid.org/0000-0002-7876-9034; Email: miljanic@uh.edu

Authors

Yun-Hsien Lin − *Department of Chemistry, University of Houston, Houston, Texas 77204-5003, United States;* orcid.org/0009-0006-0662-2697

Hayden A. Evans − *NIST Center for Neutron Research, National Institute of Standards and Technology, Gaithersburg, Maryland 20899-6102, United States;* orcid.org/0000-0002-1331-4274

Asif Raza − *Department of Chemical Sciences, Bernal Institute and Research Ireland Centre for Pharmaceuticals (SSPC), University of Limerick, Limerick V94 T9PX, Ireland*

Sousa Javan Nikkhah − *Department of Chemical Sciences, Bernal Institute and Research Ireland Centre for Pharmaceuticals (SSPC), University of Limerick, Limerick V94 T9PX, Ireland; Department of Chemistry, Maynooth University, Maynooth W23 F2H6, Ireland;* orcid.org/0000-0003-1725-4069

Xia Li − *Department of Chemical Sciences, Bernal Institute and Research Ireland Centre for Pharmaceuticals (SSPC), University of Limerick, Limerick V94 T9PX, Ireland*

Michael J. Zaworotko − *Department of Chemical Sciences, Bernal Institute and Research Ireland Centre for Pharmaceuticals (SSPC), University of Limerick, Limerick V94 T9PX, Ireland;* orcid.org/0000-0002-1360-540X
Matthias Vandichel − *Department of Chemical Sciences, Bernal Institute and Research Ireland Centre for Pharmaceuticals (SSPC), University of Limerick, Limerick V94 T9PX, Ireland;* orcid.org/0000-0003-1592-0726

Complete contact information is available at: https://pubs.acs.org/10.1021/jacs.5c16526

Author Contributions

#Y.-H.L. and H.A.E. contributed equally to this work.

Notes

The authors declare no competing financial interest.

■ ACKNOWLEDGMENTS

This work was generously supported by the US National Science Foundation (grant CHE-2204236 to O.Š.M.), the Welch Foundation (grant E-2205-20240404 to O.Š.M.), and the Research Corporation for Science Advancement (SEED grant to O.Š.M.). This research was partially supported by the NIST Center for Neutron Research (H.A.E.), and used resources of the NSLS II, U.S. Department of Energy (DOE) Office of Science User Facilities operated for the DOE Office of Science by Brookhaven National Laboratory under contract no. DESC0012704. S.M. thanks the Research Ireland Pathway grant award 21/PATH-S/9454, and the SSPC (Research Ireland Centre for Pharmaceuticals) Reward funding AzAds. M.J.Z. thanks the Research Ireland (21/US/3760) and the European Research Council (ADG 885695) grant awards. S.J.N. and M.V. thank the Irish Centre for High-End Computing (ICHEC) for the provision of computational facilities and support. S.J.N. and M.V. acknowledge support from the European Union's Horizon 2020 research and innovation programme under the Marie Skłodowska-Curie grant agreement 847402 (ID: MF20210297) and Research Ireland (23/FFP-A/12221).

■ REFERENCES

(1) (a) International Energy Agency. www.iea.org/energy-system/industry/chemicals (accessed Aug 13, 2025). (b) Moncef, Hadhri. Facts & Figures of the European Chemical Industry, cefic.org/facts-and-figures-of-the-european-chemical-industry (accessed Aug 13, 2025).
(2) Sholl, D. S.; Lively, R. P. Seven Chemical Separations to Change the World. *Nature* **2016**, *532*, 435−437.
(3) (a) Gao, M.; Song, B.; Sensharma, D.; Zaworotko, M. J. Crystal Engineering of Porous Coordination Networks for C3 Hydrocarbon Separation. *SmartMat* **2021**, *2*, 38−55. (b) Barnett, B. R.; Gonzalez, M. I.; Long, J. R. Recent Progress Towards Light Hydrocarbon Separations Using Metal-Organic Frameworks. *Trends Chem.* **2019**, *1*, 159−171.
(4) Li, L.; Lin, R.-B.; Krishna, R.; Wang, X.; Li, B.; Wu, H.; Li, J.; Zhou, W.; Chen, B. Flexible−Robust Metal−Organic Framework for Efficient Removal of Propyne from Propylene. *J. Am. Chem. Soc.* **2017**, *139*, 7733−7736.
(5) Wang, Z.; Zhang, Y.; Liu, J.; Ting Wang, T.; Wang, J.; Yu, K.; Chen, Y.; Cheng, P.; Zhang, Z. Unveiling the Flexible−Robust Feature of a Porous Organic Cage Crystal for Acetylene Separation. *ACS Mater. Lett.* **2023**, *5*, 2754−2759.
(6) Jin, F.; Lin, E.; Wang, T.; Geng, S.; Hao, L.; Zhu, Q.; Wang, Z.; Chen, Y.; Cheng, P.; Zhang, Z. Rationally Fabricating Three-Dimensional Covalent Organic Frameworks for Propyne/Propylene Separation. *J. Am. Chem. Soc.* **2022**, *144*, 23081−23088.
(7) (a) Suo, X.; Pan, H.; Chen, L.; Cui, X.; Xing, H. Control of Functionalized Pore Environment in Robust Ionic Ultramicroporous Polymers for Efficient Removal of Trace Propyne from Propylene. *ACS Appl. Mater. Interfaces* **2021**, *13*, 42706−42714. (b) Suo, X.; Cui, X.; Yang, L.; Xu, N.; Huang, Y.; He, Y.; Dai, S.; Xing, H. Synthesis of Ionic Ultramicroporous Polymers for Selective Separation of Acetylene from Ethylene. *Adv. Mater.* **2020**, *32*, No. 1907601.
(8) (a) Martínez-Fernández, M.; Hartmann, Y.; Schmidt, B. M. Porous Organic Cages as Building Blocks for Framework Materials. *Angew. Chem., Int. Ed.* **2025**, *64*, No. e202509618. (b) Yang, X.; Ullah, Z.; Stoddart, J. F.; Yavuz, C. T. Porous Organic Cages. *Chem. Rev.* **2023**, *123*, 4602−4634. (c) Robles, A.; Miljanić, O. Š. Emerging Applications of Nanoporous Molecular Crystals. *ACS Appl. Nano Mater.* **2023**, *6*, 15331−15346. (d) Little, M. A.; Cooper, A. I. The Chemistry of Porous Organic Molecular Materials. *Adv. Funct. Mater.* **2020**, *30*, No. 1909842. (e) Cooper, A. I. Porous Molecular Solids and Liquids. *ACS Cent. Sci.* **2017**, *3*, 544−553.
(9) (a) Ji, Q.; Le, H. T. M.; Wang, X.; Chen, Y.-S.; Makarenko, T.; Jacobson, A. J.; Miljanić, O. Š. Cyclotetrabenzoin: Facile Synthesis of a Shape-Persistent Molecular Square and Its Assembly into Hydrogen-Bonded Nanotubes. *Chem. - Eur. J.* **2015**, *21*, 17205−17209. See also: (b) Alrayyani, M.; Miljanić, O. Š. Benzoins and Cyclobenzoins in Supramolecular and Polymer Chemistry. *Chem. Commun.* **2018**, *54*, 11989−11997. (c) Ji, Q.; Do, L. H.; Miljanić, O. Š. Cyclotribenzoin. *Synlett* **2015**, *26*, 1625−1627.
(10) McHale, C. M.; Stegemoller, C. R.; Hashim, M. I.; Wang, X.; Miljanić, O. Š. Porosity and Guest Inclusion in Cyclobenzoin Esters. *Cryst. Growth Des.* **2019**, *19*, 562−567.
(11) Yen, Y.-J.; Chen, T.-H.; Wang, Y.-T.; Robles, A.; Đerić, M.; Miljanić, O. Š.; Kaveevivitchai, W.; Chung, S.-H. Selective Chemisorption of Polysulfides by Porous Molecular Crystal: Cathode Host Materials for Lean-electrolyte Lithium-sulfur Cells with High Electrochemical Stability. *J. Power Sources* **2023**, *565*, No. 232891.
(12) Wang, Y.-T.; McHale, C.; Wang, X.; Chang, C.-K.; Chuang, Y.-C.; Kaveevivitchai, W.; Miljanić, O. Š.; Chen, T.-H. Cyclotetrabenzoin Acetate: A Macrocyclic Porous Molecular Crystal for CO_2 Separations by Pressure Swing Adsorption. *Angew. Chem., Int. Ed.* **2021**, *60*, 14931−14937.
(13) Wang, Y.-T.; Jalife, S. J.; Robles, A.; Đerić, M.; Wu, J. I.; Kaveevivitchai, W.; Miljanić, O. Š.; Chen, T.-H. Efficient CO_2/CO Separation by Pressure Swing Adsorption Using an Intrinsically Porous Molecular Crystal. *ACS Appl. Nano Mater.* **2022**, *5*, 14021−14026.
(14) McHale, C. M.; Karas, L. J.; Wang, X.; Wu, J. I.; Miljanić, O. Š. Cyclobenzoin Esters as Hosts for Thin Guests. *Org. Lett.* **2021**, *23*, 2253−2257.
(15) For a review, see: Li, X.; Mukherjee, S.; Zaworotko, M. J. Crystal Engineering of Reticular Materials for Gas- and Liquid-phase Hydrocarbon Separation, submitted.
(16) (a) Oschatz, M.; Antonietti, M. A Search for Selectivity to Enable CO_2 Capture with Porous Adsorbents. *Energy Environ. Sci.* **2018**, *11*, 57−70. (b) Sircar, S. Basic Research Needs for Design of Adsorptive Gas Separation Processes. *Ind. Eng. Chem. Res.* **2006**, *45*, 5435−5448.
(17) (a) Krishna, R.; van Baten, J. M. How Reliable Is the Ideal Adsorbed Solution Theory for the Estimation of Mixture Separation Selectivities in Microporous Crystalline Adsorbents? *ACS Omega* **2021**, *6*, 15499−15513. (b) Fraux, G.; Boutin, A.; Fuchs, A. H.; Coudert, F.-X. On the Use of the IAST Method for Gas Separation Studies in Porous Materials with Gate-opening Behavior. *Adsorption* **2018**, *24*, 233−241.
(18) Evans, H. A.; Yildirim, T.; McCarver, G. A.; Mai, T. T.; Cheng, Y.; Deng, Z.; Klein, R. A.; Zhao, D.; Canepa, P.; Hight, A. R.; Cheetham, A. K.; Brown, C. M. Temperature-Regulated Gating Enables Gas Separations in Ultramicroporous Aluminum Formate. *ALF. Chem. Mater.* **2025**, *37*, 7102−7114.

(19) Kumar, N.; Mukherjee, S.; Harvey-Reid, N. C.; Bezrukov, A. A.; Tan, K.; Martins, V.; Vandichel, M.; Pham, T.; van Wyk, L. M.; Oyekan, K.; Kumar, A.; Forrest, K. A.; Patil, K. M.; Barbour, L. J.; Space, B.; Huang, Y.; Kruger, P. E.; Zaworotko, M. J. Breaking the Trade-off between Selectivity and Adsorption Capacity for Gas Separation. *Chem.* **2021**, *7*, 3085−3098.

(20) (a) Nikolayenko, V. I.; Castell, D. C.; Sensharma, D.; Shivanna, M.; Loots, L.; Forrest, K. A.; Solanilla-Salinas, C. J.; Otake, K.-i.; Kitagawa, S.; Barbour, L. J.; Space, B.; Zaworotko, M. J. Reversible Transformations Between the Non-Porous Phases of a Flexible Coordination Network Enabled by Transient Porosity. *Nat. Chem.* **2023**, *15*, 542−549. (b) Krause, S.; Hosono, N.; Kitagawa, S. Chemistry of Soft Porous Crystals: Structural Dynamics and Gas Adsorption Properties. *Angew. Chem., Int. Ed.* **2020**, *59*, 15325−15341.

https://doi.org/10.1021/jacs.5c16526
J. Am. Chem. Soc. 2025, 147, 43957−43963